Spatial inhomogeneities in ionic liquids, charged proteins, and charge stabilized colloids from collective variables theory

O. Patsahan
Institute for Condensed Matter Physics of the National Academy of Sciences of Ukraine, 1 Svientsitskii Str., 79011 Lviv, Ukraine

A. Ciach
Institute of Physical Chemistry, Polish Academy of Sciences, 01-224 Warszawa, Poland

(Received 11 July 2012; published 17 September 2012)

Effects of size and charge asymmetry between oppositely charged ions or particles on spatial inhomogeneities are studied for a large range of charge and size ratios. We perform a stability analysis of the primitive model of ionic systems with respect to periodic ordering using the collective variables–based theory. We extend previous studies [Ciach *et al*., Phys. Rev. E **75**, 051505 (2007)] in several ways. First, we employ a nonlocal approximation for the reference hard-sphere fluid which leads to the Percus-Yevick pair direct correlation functions for the uniform case. Second, we use the Weeks-Chandler-Anderson regularization scheme for the Coulomb potential inside the hard core. We determine the relevant order parameter connected with the periodic ordering and analyze the character of the dominant fluctuations along the λ lines. We show that the above-mentioned modifications produce large quantitative and partly qualitative changes in the phase diagrams obtained previously. We discuss possible scenarios of the periodic ordering for the whole range of size and charge ratios of the two ionic species, covering electrolytes, ionic liquids, charged globular proteins or nanoparticles in aqueous solutions, and charge-stabilized colloids.

DOI: 10.1103/PhysRevE.86.031504 PACS number(s): 61.20.Qg

I. INTRODUCTION

The study of phase diagrams of ionic systems in which the phase separation is mainly driven by electrostatic forces is of great fundamental interest and practical importance. Electrolyte solutions, molten salts, ionic liquids, and charge stabilized colloidal suspensions are examples of systems with dominant Coulomb interactions. The strong correlations between ions and counterions are also known to play an important role in determining structure and phase behavior of micelles, polyelectrolytes, and proteins. Over the past few decades, the phase behavior of ionic fluids has been the subject of many experimental, theoretical, and simulation studies and the reviews of the state of the art in this field are available in Refs. [1–6]. A great deal of the research has been focused on the fluid-fluid phase separation, whereas the fluid-solid phase transition has received less attention so far.

On the other hand, recent experimental, simulation and theoretical studies of room-temperature ionic liquids (RTILs) [7], charged globular proteins [8,9], or colloidal particles [8,10–14] reveal structural inhomogeneities of different types and spatial extents, and it becomes evident that the ordering in systems dominated by Coulomb interactions has a very rich and complex nature and is far from being understood. Consequently, ordering of ions or charged particles on different length scales is attracting increasing attention.

The much-studied simple salts or electrolytes are quite well understood. In these systems, the sizes of ions are similar. Therefore, theoretical studies focused mainly on the restricted primitive model (RPM) where ions of the same valence are modeled by charged hard spheres of the same diameter immersed in a structureless dielectric continuum (either vacuum or solvent). At large-enough volume fractions, transition to an ionic crystal occurs in molten salts when temperature decreases [15–18]. In the ionic crystal the charge is periodically ordered and this ordering is subjected to the charge neutrality. On the other hand, charge-ordered, neutral living clusters of various sizes and lifetimes were found in simulation studies of the fluid phase [19–23].

A direct inspection of the structure in ionic systems is complicated due to a small size of the ions. However, in compliance with the law of corresponding states, one may expect a similar behavior in oppositely charged colloidal particles of similar sizes under appropriate rescaling of the length and energy units. The natural length scale is the sum of radii of the anion and the cation, $\sigma_{\pm}$, while the energy unit is the Coulomb potential between the oppositely charged ions at contact, $E_0 = q_+q_-/(\epsilon\sigma_{\pm})$, where q_α is the charge of the α-type ion ($\alpha = +,-$) and ϵ is the dielectric constant of the solvent. If the non-Coulomb interactions are negligible, the phase diagrams of systems consisting of spherical ions of various sizes should have the same form in terms of the volume fraction and a reduced temperature $T^* = k_BT/E_0$. Indeed, simulations show that the phase diagram of charged particles with similar sizes in deionized solvent (large Debye screening length) resembles the phase diagram of the RPM [18,24,25]. In the above reduced units, the room temperature is very low for simple salts, whereas for colloidal particles it is high. Ordering of colloids at room temperature is directly accessible to observations and vacancies in the crystal can be seen [26]. Formation of neutral aggregates in the RPM agrees with recent experimental studies of oppositely charged proteins of similar sizes [9,27]. The aggregation was entirely suppressed when the electrostatic interactions had been screened by addition of a sufficient amount of salt. Thus, the electrostatic interaction is essential at least for the first step of the self-assembly of oppositely charged globular proteins into aggregates. Large

spherical aggregates presumably indicate nucleation of a crystal.

RTILs differ from simple salts mainly because the sum of radii of the ions is much larger. This reduces the strength of the Coulomb interactions at ion contact and, in turn, increases the room temperature in the reduced units. In addition, in many RTILs the size and shape of the anion can differ substantially from the size and shape of the cation. Moreover, non-Coulomb interactions may play an important role here. In such a case, the RPM is an oversimplification, and the above discussion does not apply to the RTILs. Recent experimental and simulation studies on a series of imidazolium-based RTILs indicate spatial inhomogeneities on a length scale of $\sim$10 nm [7]. The inhomogeneous structure of liquid resembles the structure of the crystal [7]. The origin of such nanoheterogeneity has not been convincingly explained yet, and new studies are required.

In a mixture of positively and negatively charged globular proteins, the size difference between the positively and negatively charged molecules can be similar to the size difference between the anion and the cation in the RTILs. Recent experimental studies show that the size difference plays an important role for the assembly of proteins into aggregates. According to Ref. [9], formation of spherical aggregates of oppositely charged proteins with overall charge near zero requires charge and size compensation.

The size difference between charged globular proteins and counterions in a solution is much larger than in the previously described cases. For example, the diameter of a lysozyme molecule is of the order of 3 nm, i.e., it is 10 times larger than the counterions in an aqueous solution. The charge of small globular proteins is of the order of $10e$, where e is the elementary charge. Scattering experiments [8] suggest clustering of protein molecules in water. Effective interactions between the lysozyme molecules were shown to have a form of short-range attraction and long-range repulsion—the latter resulting from the charges on the molecules [28]. The effective attraction between two molecules is caused by the interactions between them and the counterions attracted to both molecules, as well as by the non-Coulomb forces. Simulations carried out in Ref. [29] for the potential derived in Ref. [28] show that the fraction of clustered molecules and the shape of clusters strongly depend on the lysozyme volume fraction.

Charged nanoparticles or colloidal particles with a diameter of $\sim$10–1000 nm are several orders of magnitude larger than the microscopic counterions in a solution, and their charge can be orders of magnitude larger than the charge of the counterion. In these systems, the experiments indicate the formation of colloidal crystals with large interparticle distance for small volume fractions and a re-entrant melting for larger volume fractions [10,11,13].

From the above description of different experimental systems it follows that spatial inhomogeneities are common, but their extent and nature still need to be comprehended and classified for different sizes and charges of the anion and the cation. In the first step, it is essential to predict the structure formation and phase diagram for various size and charge ratios for a generic model where non-Coulomb interactions, deviations from a spherical shape, and flexibility of molecules are neglected. The above factors have been taken into account in the recent theoretical and simulation studies focusing on the structure and phase behavior of complex systems of charged components, e.g., ionic liquid crystals [30–32]. In this work we limit ourselves to nearly spherical, stiff ions or particles with negligible non-Coulomb forces.

The generic model that allows one to predict the phase separation driven exclusively by Coulomb forces is a primitive model (PM). In this model, the ionic fluid is described as an electroneutral mixture of charged hard spheres immersed in a structureless dielectric continuum. The PM pair potential for two ions α and β at distance r apart is

$$U_{\alpha\beta}(r) = \begin{cases} \infty, & r < \sigma_{\alpha\beta} \\ \frac{q_\alpha q_\beta}{\epsilon r}, & r \geqslant \sigma_{\alpha\beta} \end{cases}, \tag{1}$$

where an ion of species α has a diameter σ_α, charge q_α, $\sigma_{\alpha\beta} = \frac{1}{2}(\sigma_\alpha + \sigma_\beta)$, and ϵ is the dielectric constant. The PM is the simplest model for all the above-discussed systems. The two-component PM can be characterized by the parameters of size and charge asymmetry as follows:

$$\lambda = \frac{\sigma_+}{\sigma_-}, \quad Z = \frac{q_+}{|q_-|}. \tag{2}$$

For $\lambda = Z = 1$ one arrives at the RPM.

In the PM with a large difference in the ion radii, the spatial distribution of the ions is expected to differ markedly from the RPM, because the tendency for minimizing the electrostatic energy competes with the geometrical restriction on packing of spheres with different sizes [26]. Packing of large and small spheres that maximizes the entropy could lead to the formation of mesoscopic charged regions, and, on the other hand, when the electrostatic energy is minimized, periodic pattern involving voids could be formed. As a result of the competition between maximizing entropy and minimizing energy, both the charge and the number density of ions can oscillate in space.

The systematic studies of the effects of size and charge asymmetry on the periodic ordering in PMs were initiated in Ref. [33] within the framework of the field theoretical description. Based on a mean-field stability analysis, the authors found the boundaries of stability of the disordered phase for the whole range of λ and Z. It was shown that, besides a gas-liquid separation, in a certain portion of the phase diagram, the uniform fluid became unstable with respect to the order parameter oscillations of wavelengths $2\pi/k_b$ with $k_b \neq 0$. The line in the phase diagram corresponding to the instability of the disordered phase with respect to periodic ordering is called the λ line [34] to distinguish it from the spinodal line for which $k_b = 0$. The results obtained in Ref. [33] show that (i) the periodic ordering mainly depends on the size asymmetry and (ii) the qualitative dependence on the charge asymmetry is found only for a sufficiently large size asymmetry.

In this paper, we continue the systematic study of the periodic ordering in asymmetric PMs. We extend the previous study in several ways. The first modification concerns an approximate description of the reference hard-sphere mixture. In Ref. [33] a local-density approximation is employed for a hard-sphere free-energy functional. Here, we consider a nonlocal approximation for the reference hard-sphere fluid which is shown to lead to the Percus-Yevick (PY) theory for the

uniform case [35]. In our calculations we use the Lebowitz's solution of the generalized PY equation [36].

Another modification concerns the regularization of the Coulomb potential inside the hard core. It is worth noting that in the treatments of models with hard cores, the perturbation potential is not defined uniquely inside the hard core. Here we use the Weeks-Chandler-Andersen (WCA) regularization scheme for the Coulomb potentials $\phi^C_{\alpha\beta}(r)$ [37]

$$\phi^C_{\alpha\beta}(r) = \begin{cases} \frac{q_\alpha q_\beta}{\epsilon\sigma_{\alpha\beta}}, & r < \sigma_{\alpha\beta} \\ \frac{q_\alpha q_\beta}{\epsilon r}, & r \geqslant \sigma_{\alpha\beta} \end{cases} \tag{3}$$

instead of $\phi^C_{\alpha\beta}(r) = q_\alpha q_\beta \theta(r-\sigma_{\alpha\beta})/(\epsilon r)$ adopted in Ref. [33]. As was shown in Ref. [38], the simple form for $\phi^C_{\alpha\beta}(r)$ given in Eq. (3) produces rapid convergence of the series of the perturbation theory for the free energy. On the other hand, the best theoretical estimates for the gas-liquid critical point of the RPM was obtained using the WCA regularization scheme [39].

Finally, we extend the study of the relevant order parameter (OP) undertaken in Ref. [33]. Following the ideas of Refs. [40,41], we determine the OP connected with the phase transition to an ordered phase and analyze the character of the dominant fluctuations along the λ lines associated with the periodic ordering.

A theoretical background for this study is the statistical field theory that exploits the method of collective variables (CVs) [42–45]. The theory enables us to derive an exact expression for the functional of grand partition function (GPF) of the model and, on this basis, to develop the perturbation theory [45–47]. As was shown in Ref. [47], the well-known approximations for the free energy, in particular Debye-Hückel limiting law and the mean spherical approximation, can be reproduced within the framework of this theory. Links between this approach and the field theoretical approach [33] were established in Ref. [48] for the case of the RPM.

Our paper is organized as follows. In Sec. II we give some brief background to the CVs-based theory for the PM. Based on the Gaussian approximation of the functional of GPF we obtain the pair direct correlation functions and determine the OP characterizing the periodic ordering in PMs. In Sec. III we study the effects of size and charge asymmetry on the periodic ordering taking into account the above-listed modifications. We discuss the results in Sec. IV and conclude in Sec. V.

II. THEORETICAL BACKGROUND

A. Functional representation

We start with the general case of a two-component PM consisting of N_+ cations carrying a charge $q_+ = Zq$ of diameter σ_+ and N_- anions carrying a charge $q_- = -q$ of diameter σ_-. The ions are immersed in a structureless dielectric continuum (either vacuum or solvent). The system is electrically neutral: $\sum_{\alpha=+,-} q_\alpha \rho_\alpha = 0$ and $\rho_\alpha = N_\alpha/V$ is the number density of the αth species.

The pair interaction potential is assumed to be of the following form:

$$U_{\alpha\beta}(r) = \phi^{\rm HS}_{\alpha\beta}(r) + \phi^{\rm C}_{\alpha\beta}(r), \tag{4}$$

where $\phi^{\rm HS}_{\alpha\beta}(r)$ is the interaction potential between the two additive hard spheres of diameters σ_α and σ_β. We call the two-component hard-sphere system a reference system. Thermodynamic and structural properties of the reference system are assumed to be known. $\phi^{\rm C}_{\alpha\beta}(r)$ is the Coulomb potential given in Eq. (3), and hereafter we put $\epsilon = 1$.

Using the CV method, we get an exact functional representation of GPF for the PM with size and charge asymmetry [45],

$$\Xi[\nu_\alpha] = \int (d\rho)(d\omega) \exp\left[-\frac{\beta}{2V} \sum_{\alpha,\beta} \sum_{\mathbf{k}} \tilde{\phi}^C_{\alpha\beta}(k) \rho_{\mathbf{k},\alpha} \rho_{-\mathbf{k},\beta} + i \sum_\alpha \sum_{\mathbf{k}} \omega_{\mathbf{k},\alpha} \rho_{\mathbf{k},\alpha} + \ln \Xi_{\rm HS}[\bar{\nu}_\alpha - i\omega_\alpha] \right]. \tag{5}$$

In Eq. (5) $\rho_{\mathbf{k},\alpha} = \rho^c_{\mathbf{k},\alpha} - i\rho^s_{\mathbf{k},\alpha}$ is the CV which describes the value of the $\mathbf{k}$-th fluctuation mode of the number density of the αth species. Each of $\rho^c_{\mathbf{k},\alpha}$ ($\rho^s_{\mathbf{k},\alpha}$) takes all the real values from $-\infty$ to $+\infty$; $\omega_{\mathbf{k},\alpha}$ is conjugate to the CV $\rho_{\mathbf{k},\alpha}$; $(d\rho)$ and $(d\omega)$ are volume elements of the CV phase space

$$(d\rho) = \prod_\alpha d\rho_{0,\alpha} \prod_{\mathbf{k}\neq 0}{}' d\rho^c_{\mathbf{k},\alpha} d\rho^s_{\mathbf{k},\alpha},$$

$$(d\omega) = \prod_\alpha d\omega_{0,\alpha} \prod_{\mathbf{k}\neq 0}{}' d\omega^c_{\mathbf{k},\alpha} d\omega^s_{\mathbf{k},\alpha}$$

and the product over $\mathbf{k}$ is performed in the upper semispace ($\rho_{-\mathbf{k},\alpha} = \rho^*_{\mathbf{k},\alpha}$, $\omega_{-\mathbf{k},\alpha} = \omega^*_{\mathbf{k},\alpha}$).

$\tilde{\phi}^{\rm C}_{\alpha\beta}(k)$ is the Fourier transform of the Coulomb potential. In the case of the WCA regularization [see Eq. (3)] we obtain, for $\beta\tilde{\phi}^C_{\alpha\beta}(k)$ [46],

$$\beta\tilde{\phi}^C_{++}(k) = \frac{4\pi Z\sigma_\pm^3}{T^*(1+\delta)} \frac{\sin[x(1+\delta)]}{x^3}, \tag{6}$$

$$\beta\tilde{\phi}^C_{--}(k) = \frac{4\pi\sigma_\pm^3}{T^* Z(1-\delta)} \frac{\sin[x(1-\delta)]}{x^3}, \tag{7}$$

$$\beta\tilde{\phi}^C_{+-}(k) = -\frac{4\pi\sigma_\pm^3}{T^*} \frac{\sin(x)}{x^3}, \tag{8}$$

where the following notations are introduced:

$$T^* = \frac{k_B T}{E_0} = \frac{k_B T \sigma_\pm}{q^2 Z} \tag{9}$$

is the dimensionless temperature, $x = k\sigma_\pm$, $\sigma_\pm = (\sigma_+ + \sigma_-)/2$, and

$$\delta = \frac{\lambda - 1}{\lambda + 1}. \tag{10}$$

Similarly, hereafter we introduce the parameter ν

$$\nu = \frac{Z-1}{Z+1}. \tag{11}$$

The parameters δ and ν are more convenient than the parameters λ and Z because they vary between -1 and 1. Following Ref. [33], we choose the dimensionless temperature T^* given in Eq. (9) and the volume fraction of all ions

$$\zeta = \frac{\pi}{6}(\rho_+\sigma_+^3 + \rho_-\sigma_-^3) \tag{12}$$

as thermodynamic variables.

$\Xi_{\rm HS}[\bar{\nu}_\alpha - i\omega_\alpha]$ is the GPF of a two-component hard-sphere system with the renormalized chemical potential

$$\bar{\nu}_\alpha = \nu_\alpha + \frac{\beta}{2V}\sum_{\mathbf{k}} \tilde{\phi}^C_{\alpha\alpha}(k) \tag{13}$$

in the presence of the local field $-i\omega_\alpha(r)$. In Eq. (13) ν_α is the dimensionless chemical potential, $\nu_\alpha = \beta\mu_\alpha - 3\ln\Lambda_\alpha$, μ_α is the chemical potential of the αth species, β is the reciprocal temperature, and $\Lambda_\alpha^{-1} = (2\pi m_\alpha \beta^{-1}/h^2)^{1/2}$ is the inverse de Broglie thermal wavelength.

In order to develop the perturbation theory we present $\ln \Xi_{\rm HS}[\bar{\nu}_\alpha - i\omega_\alpha]$ in the form of the cumulant expansion

$$\ln \Xi_{\rm HS}[\ldots] = \sum_{n\geqslant 0}\frac{(-i)^n}{n!}\sum_{\alpha_1,\ldots,\alpha_n}\sum_{\mathbf{k}_1,\ldots,\mathbf{k}_n} \mathfrak{M}_{\alpha_1\ldots\alpha_n}(\bar{\nu}_\alpha;k_1,\ldots,k_n) \times\omega_{\mathbf{k}_1,\alpha_1}\ldots\omega_{\mathbf{k}_n,\alpha_n}\delta_{\mathbf{k}_1+\ldots+\mathbf{k}_n}, \tag{14}$$

where $\delta_{\mathbf{k}_1+\ldots+\mathbf{k}_n}$ is the Kronecker symbol. In Eq. (14) the nth cumulant $\mathfrak{M}_{\alpha_1\ldots\alpha_n}$ coincides with the Fourier transform of the n-particle connected correlation function of a two-component hard-sphere system [45].

B. Gaussian approximation

Having set $\mathfrak{M}_{\alpha_1\ldots\alpha_n} \equiv 0$ for $n \geqslant 3$, after integration in Eq. (5) over $\omega_{\mathbf{k},\alpha}$ one arrives at the Gaussian approximation for the functional of GPF [46]

$$\Xi_{\rm G}[\nu_\alpha] = \Xi_{\rm MF}[\bar{\nu}_\alpha]\ \Xi'\int(d\rho) \times\exp\left\{-\frac{1}{2V}\sum_{\alpha,\beta}\sum_{\mathbf{k}}\tilde{\mathcal{C}}_{\alpha\beta}(k)\rho_{\mathbf{k},\alpha}\rho_{-\mathbf{k},\beta}\right\}, \tag{15}$$

where $\Xi_{\rm MF}$ is the GPF in the mean-field (MF) approximation and $\Xi' = \prod_{\mathbf{k}}\det[V^2\mathfrak{M}_2]^{-1/2}$ with $\mathfrak{M}_2$ being the matrix of elements $\mathfrak{M}_{\alpha\beta}(k)/V$. $\tilde{\mathcal{C}}_{\alpha\beta}(k)$ is the Fourier transform of the pair direct (vertex) correlation function in the random-phase approximation (RPA),

$$\tilde{\mathcal{C}}_{\alpha\beta}(k) = \beta\tilde{\phi}^C_{\alpha\beta}(k) + \tilde{\mathcal{C}}^{\rm HS}_{\alpha\beta}(k). \tag{16}$$

In Eq. (16), $\tilde{\mathcal{C}}^{\rm HS}_{\alpha\beta}(k)$ is the Fourier transform of the pair direct correlation function of a two-component hard-sphere system. It is connected with $\mathfrak{M}_{\alpha\beta}(k)$ by the relation $\tilde{\mathcal{C}}^{\rm HS}_2(k)\mathfrak{M}_2(k) = \underline{1}$, where $\tilde{\mathcal{C}}^{\rm HS}_2(k)$ denotes the matrix of elements $\tilde{\mathcal{C}}^{\rm HS}_{\alpha\beta}(k)$ and $\underline{1}$ is the unit matrix. In the limit $k = 0$, the $\tilde{\mathcal{C}}^{\rm HS}_{\alpha\beta}$ coincides with the coefficients $a_{\alpha\beta}$ which are obtained in Ref. [33] as a result of the local-density approximation.

It is convenient to introduce CVs which describe the fluctuation modes of the total number and charge density, $\rho_{\mathbf{k},N}$ and $\rho_{\mathbf{k},Q}$, by the relations

$$\rho_{\mathbf{k},N} = \frac{1}{1+Z}(\rho_{\mathbf{k},+} + \rho_{\mathbf{k},-}),\qquad \rho_{\mathbf{k},Q} = \frac{1}{1+Z}(Z\rho_{\mathbf{k},+} - \rho_{\mathbf{k},-}). \tag{17}$$

Then, Eq. (15) can be rewritten in terms of $\rho_{\mathbf{k},N}$ and $\rho_{\mathbf{k},Q}$ as follows:

$$\Xi_{\rm G}[\nu_\alpha] = \Xi_{\rm MF}[\bar{\nu}_\alpha]\ \Xi'\int(d\rho_N)(d\rho_Q) \times\exp\left\{-\frac{1}{2V}\sum_{A,B}\sum_{\mathbf{k}}\tilde{\mathcal{C}}_{AB}(k)\rho_{\mathbf{k},A}\rho_{-\mathbf{k},B}\right\}, \tag{18}$$

where $A(B) = N, Q$ and

$$\tilde{\mathcal{C}}_{NN}(k) = \frac{1}{(1+Z)^2}[\tilde{\mathcal{C}}_{++}(k) + Z^2\tilde{\mathcal{C}}_{--}(k) + 2Z\tilde{\mathcal{C}}_{+-}(k)],$$
$$\tilde{\mathcal{C}}_{QQ}(k) = \frac{1}{(1+Z)^2}[\tilde{\mathcal{C}}_{++}(k) + \tilde{\mathcal{C}}_{--}(k) - 2\tilde{\mathcal{C}}_{+-}(k)], \tag{19}$$
$$\tilde{\mathcal{C}}_{QN}(k) = \frac{1}{(1+Z)^2}[\tilde{\mathcal{C}}_{++}(k) - Z\tilde{\mathcal{C}}_{--}(k) + (Z-1)\tilde{\mathcal{C}}_{+-}(k)]$$

are the density-density, charge-charge, and charge-density direct correlation functions, respectively.

In general, an equation for the boundary of stability of the uniform phase with respect to fluctuations is given by

$$\det\tilde{\mathcal{C}}_2|_{k=k_b} = 0, \tag{20}$$

where $\tilde{\mathcal{C}}_2$ denotes the matrix of elements $\tilde{\mathcal{C}}_{AB}(k)$ [or $\tilde{\mathcal{C}}_{\alpha\beta}(k)$]. The corresponding wave vector k_b is determined from the equation [34]

$$\partial\det\tilde{\mathcal{C}}_2/\partial k = 0. \tag{21}$$

The case $k = k_b = 0$ corresponds to the gas-liquid-like separation [33,46]. Here we are interested in the λ line, the boundary of stability associated with fluctuations of the OP with $k = k_b \neq 0$. On the λ line, the fluid becomes unstable with respect to the periodic ordering, indicating that there can be a phase transition to an ordered phase.

The first-order transitions between the disordered and ordered phases can be determined beyond the Gaussian approximation discussed in this section. In the case of colloid particles the transitions between different crystal phases were obtained in MF for short-range attraction long-range repulsion effective interactions that are supposed to include counterion-mediated contribution. The transition between the disordered and periodic phases was found to be located close to the λ line [49,50]. In the case of the RPM, we have shown, using field-theoretic methods, that beyond MF a first-order transition to ionic crystal occurs for volume fractions much higher than at the λ line [16]. In both studies the local density approximation for the reference system was assumed in an approach analogous to a simplified version of the present theory (like in Ref. [33]). The present nonlocal approximation (with included cumulants up to the fourth order) should yield a more accurate description of phase coexistence especially for the RPM, since for a small distance between the ions in a crystal the local density approximation is an oversimplification. Studies beyond the Gaussian approximation go beyond the scope of this work, however.

C. Order parameter

The determination of the OP is the important issue in the phase transition theory of mixtures. This problem has got a consistent and clear solution within the given approach.

In order to determine the OP associated with the periodic ordering, we follow the ideas of Refs. [40,41]. First, we diagonalize the square form in Eq. (18) by means of an orthogonal transformation

$$\xi_{\mathbf{k},1} = t_{NN}\rho_{\mathbf{k},N} + t_{NQ}\rho_{\mathbf{k},Q}, \tag{22}$$

$$\xi_{\mathbf{k},2} = t_{QN}\rho_{\mathbf{k},N} + t_{QQ}\rho_{\mathbf{k},Q}. \tag{23}$$

The explicit expression for coefficients t_{AB} are given in the appendix. The corresponding eigenvalues $\varepsilon_1(k)$ and $\varepsilon_2(k)$ are found to be

$$\varepsilon_{1,2}(k) = \tfrac{1}{2}\big(\tilde{\mathcal{C}}_{NN}(k) + \tilde{\mathcal{C}}_{QQ}(k) \pm \big\{[\tilde{\mathcal{C}}_{NN}(k) - \tilde{\mathcal{C}}_{QQ}(k)]^2 + 4\tilde{\mathcal{C}}^2_{NQ}(k)\big\}^{1/2}\big). \tag{24}$$

Based on the solutions of Eqs. (20) and (21), we find the eigenvalue which becomes equal to zero along the calculated λ lines for the fixed values of parameters δ and ν. We suggest that the corresponding eigenmode is connected with the relevant OP.

Our analysis shows that only one of the eigenvalues, i.e., $\varepsilon_2(k)$, becomes zero along the λ line of both the symmetric and asymmetric PMs. The same result was obtained earlier for a mixture of neutral particles [40,41]. In Figs. 1 and 2 we show typical behavior of $\varepsilon_1(k)$ and $\varepsilon_2(k)$ under thermodynamic conditions corresponding to the points located on the λ lines associated with $k_b \neq 0$.

We assume that CV $\xi_{\mathbf{k},2}$ is connected to the relevant OP. Based on Eqs. (22) and (23), we can determine the direction of strong fluctuations along the λ line by the relation

$$\tan\theta = \frac{t_{NQ}}{t_{NN}} = -\frac{t_{QN}}{t_{QQ}}, \tag{25}$$

where θ is the rotation angle of axes $\xi_{\mathbf{k}_b,1}$ and $\xi_{\mathbf{k}_b,2}$ in the plane $(\rho_{\mathbf{k}_b,N},\rho_{\mathbf{k}_b,Q})$. The case $\theta = 0$ corresponds to the pure charge density fluctuations (axes $\xi_{\mathbf{k}_b,2}$ and $\rho_{\mathbf{k}_b,Q}$ coincide) and the case $\theta = \mp\pi/2$ corresponds to the pure total number density fluctuations (axis $\xi_{\mathbf{k}_b,2}$ coincides with axes $\pm\rho_{\mathbf{k}_b,N}$, respectively). Taking into account the formulas from the appendix [Eqs. (A1)–(A4)], we have

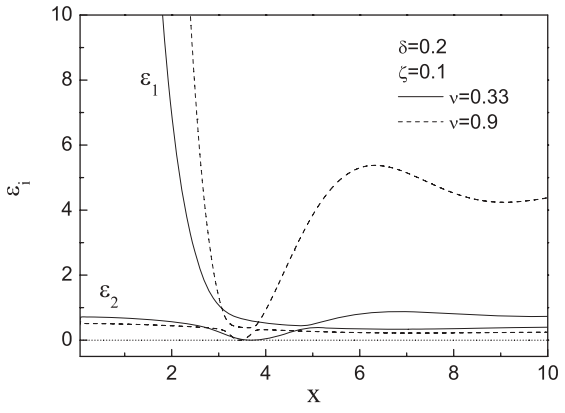

FIG. 1. PM with a small size asymmetry ($\delta = 0.2$): the dependence of eigenvalues ε_1 and ε_2 on the wave numbers ($x = k\sigma_+$). Solid and dashed lines correspond to $\nu = 0.33$ ($\zeta = 0.1$, $T^* \simeq 0.033$) and $\nu = 0.9$ ($\zeta = 0.1$, $T^* \simeq 0.068$), respectively.

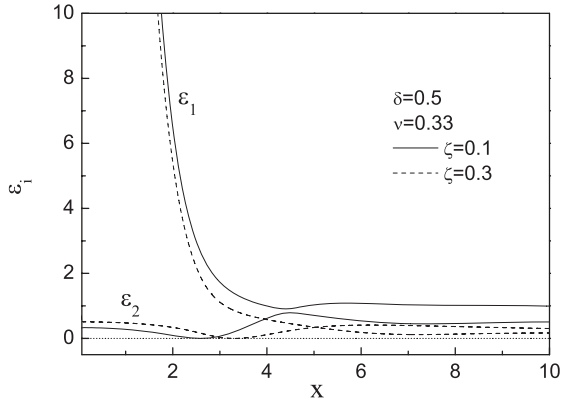

FIG. 2. PM with a moderate size asymmetry ($\delta = 0.5$, $\nu = 0.33$): the dependence of eigenvalues ε_1 and ε_2 on the wave numbers ($x = k\sigma_+$). The solid and dashed lines correspond to $\zeta = 0.1$, $T^* \simeq 0.033$ and $\zeta = 0.3$, $T^* \simeq 0.037$, respectively.

$$\tan\theta = -\frac{1}{\alpha_2} = \alpha_1. \tag{26}$$

It is worth noting that, in the long-wavelength limit, $\alpha_2(k = 0) = 0$, and one gets $\theta = -\pi/2$, in agreement with the expected separation into homogeneous charge neutral dilute and dense phases.

In Ref. [33] the analysis was similar, except that the eigenvalues denoted by $\tilde{C}_{\phi\phi}(k)$ and $\tilde{C}_{\eta\eta}(k)$ were defined directly in terms of $\tilde{C}_{\alpha\beta}$ in such a way that $\varepsilon_2(k) = \tilde{C}_{\phi\phi}(k)$ when $\tilde{C}_{+-}(k) > 0$ and $\varepsilon_2(k) = \tilde{C}_{\eta\eta}(k)$ when $\tilde{C}_{+-}(k) < 0$. $\tilde{C}_{\phi\phi}(k)$ and $\tilde{C}_{\eta\eta}(k)$, defined in Ref. [33], reduce to the direct correlation functions for the charge and for the number density, respectively, for $Z = 1$ (i.e., for the RPM), and the corresponding eigenmodes reduce, for $Z = 1$, to the charge and the number density waves. The advantage of the present approach is that the critical mode is associated with the same eigenvalue $\varepsilon_2(k)$ independently of k, ζ, and T. It is also more convenient to present the nature of the eigenmode in terms of the angle θ rather than in terms of the parameter R introduced in Ref. [33] in a way analogous to $\tan\theta$ in Eq. (25).

III. BOUNDARY OF STABILITY ASSOCIATED WITH PERIODIC ORDERING: RANDOM-PHASE APPROXIMATION

In this section we study the effects of size and charge asymmetry on the boundary of stability against the fluctuations with $k = k_b \neq 0$. To this end, we use Eqs. (20) and (21) taking into account Eqs. (6)–(8). In order to determine the character of the dominant fluctuations we use Eq. (25).

We take into account the k dependence of the direct correlation functions of the reference system using an exact solution of the generalized PY equation obtained by Lebowitz [36]. The explicit expressions for the Fourier transforms of the OZ partial direct correlation functions of a two-component hard sphere system are given in Refs. [51,52]. They are too cumbersome to be reproduced here.

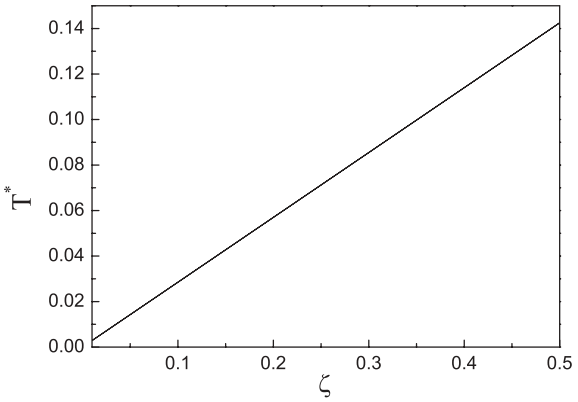

FIG. 3. The λ line for the transition to the ordered phase for $\delta = 0$. Temperature T^* and the volume fraction of ions ζ are in dimensional reduced units defined in Eqs. (9) and (12), respectively.

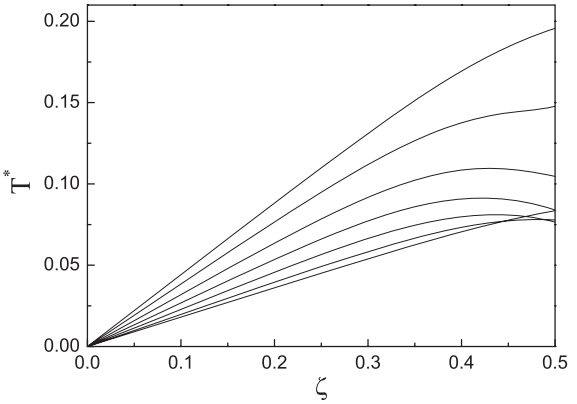

FIG. 4. The λ lines for the transition to the ordered phase for $\delta = 0.1$ ($\nu \geqslant 0$ and $\nu < 0$). Lines from the top to the bottom: $\nu = 0.9$, $\nu = 0.67$, $\nu = 0.33$, $\nu = 0$, $\nu = -0.33$, $\nu = -0.67$, $\nu = -0.9$. Temperature T^* and the volume fraction of ions ζ are in dimensional reduced units defined in Eqs. (9) and (12), respectively.

As in Ref. [33], we distinguish the three regimes in size asymmetry: small size asymmetry, moderate and large size asymmetry, and very large size and charge asymmetry. Each regime is characterized by a typical behavior of the λ lines. As we will see below, the δ ranges of these regimes slightly differ when compared to Ref. [33]. We also dwell briefly on the size-symmetric case.

A. Size-symmetric PM

We start with a size-symmetric PM corresponding to $\delta = 0$ (or $\lambda = 1$). In Fig. 3 the λ line associated with the wave vector $k_b \neq 0$ is displayed. As is seen, it is a straight line identical to that obtained for the RPM [53,54]: $T^*(k = k_b) = S_\lambda \zeta$. For the WCA regularization, $S_\lambda \simeq 0.285$ and $x_b = k_b \sigma_\pm = k_b \sigma \simeq 4.078$ [54].

For the size-symmetric PM, the angle θ indicating the direction of the strong fluctuations is equal to zero. Therefore, the λ line shown in Fig. 3 is the boundary of stability of the uniform phase against the charge density fluctuations.

The charge asymmetry has no effect on the λ line of the size-symmetric PM. This property does not persist if the higher-order terms are taken into account in Eq. (14) (see Refs. [47,55,56]). The effects of charge-density fluctuations on a phase behavior of RPM ($\delta = 0$, $\nu = 0$) were studied in Ref. [16] using the field theoretical description. It was found that in the presence of fluctuations, the λ line disappears. Instead, a fluctuation-induced first-order transition to an ionic crystal appears. Interestingly, the wavelength of the charge wave is independent of the density along the liquid-crystal coexistence line [16], which was interpreted as the formation of vacancies in the crystal of a fixed unit cell when the density of ions decreases. We expect the similar situation to take place for the PM with the small size asymmetry.

B. Small size asymmetry

Now we consider the asymmetric PMs with a small size asymmetry ($\delta < 0.3$ or $\lambda < 2$). This case corresponds to molten salts, electrolytes, some RTILs, and oppositely charged globular protein or nanoparticle mixtures in the limit of infinite screening length. The λ lines associated with the wave vectors $k_b \neq 0$ are shown in Fig. 4 for $\delta = 0.1$. It should be noted that the λ lines are located at the temperatures that are an order of magnitude lower than those in Ref. [33]. In addition, the monotonously increasing behavior of the λ-line temperature, T^* versus ζ, is found for a sufficiently large charge asymmetry ($|\nu| > 0.33$). For $|\nu| \leqslant 0.33$, T^* has a maximum in the range $\zeta \simeq 0.42$–0.48. The effect comes into prominence with an increase of δ. This differs from the previous results [33] demonstrating a monotonous increase of T^* with ζ along the λ lines ($\zeta = 0$–0.7) for all ν. The difference is directly related to the nonlocal approximation for the reference hard-sphere system adopted in the present work. As is seen from Fig. 4, the λ-line temperature increases when ν increases from -0.9 to 0.9, which qualitatively agrees with Ref. [33].

For a small size asymmetry, the wave numbers characterizing the period of the OP oscillations in a nonuniform phase are $x_b = k_b \sigma_\pm > \pi$ and their magnitudes depend very slightly on ζ (see Fig. 5). The comparison with Ref. [33] implies that the magnitude of x_b is mainly determined by the regularization method of the Coulomb potential inside the hard core. In Fig. 5 we also demonstrate the effect of charge asymmetry on x_b. As

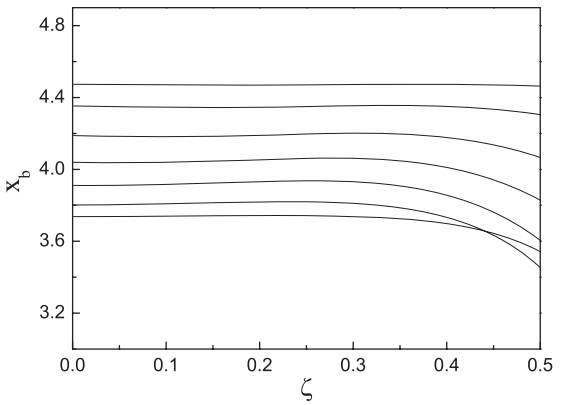

FIG. 5. The wave number $x_b = k_b \sigma_\pm$ corresponding to the ordering of ions along the λ lines shown in Fig. 4 for $\delta = 0.1$ ($\nu \geqslant 0$ and $\nu < 0$). Lines from the bottom to the top: $\nu = 0.9$, $\nu = 0.67$, $\nu = 0.33$, $\nu = 0$, $\nu = -0.33$, $\nu = -0.67$, $\nu = -0.9$. ζ is the volume fraction of ions.

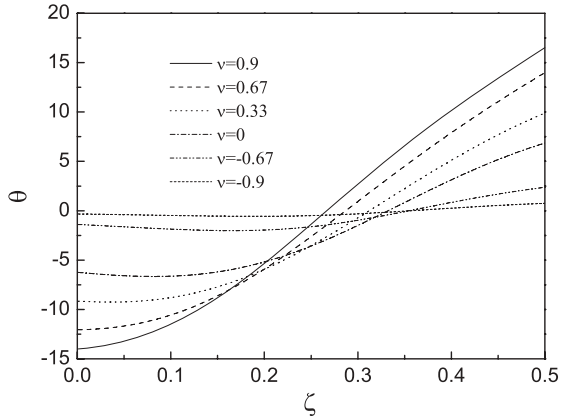

FIG. 6. The variation of the angle θ along the λ lines presented in Fig. 4 ($\nu \geqslant 0$ and $\nu < 0$). θ is measured in degrees.

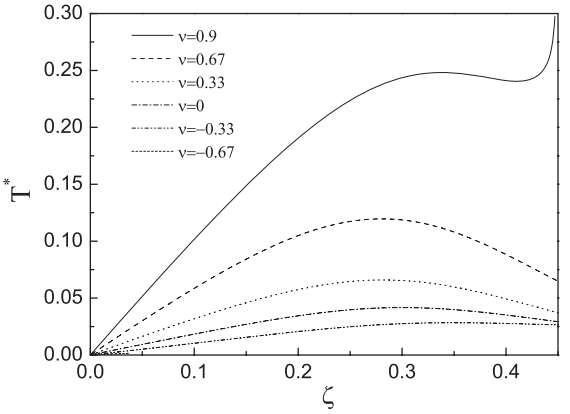

FIG. 7. The λ lines for the transition to the ordered phase for $\delta = 0.3$ ($\nu \geqslant 0$ and $\nu < 0$). Temperature T^* and the volume fraction of ions ζ are in dimensional reduced units defined in Eqs. (9) and (12), respectively. The curve for $\nu = -0.67$ is located at a very low temperature and is indistinguishable in this plot.

is seen, x_b increases with the variation of ν from 0.9 to -0.9 for the fixed ζ, which agrees with the results obtained in Ref. [33].

We have calculated the angle θ showing the direction of strong fluctuations along the λ line. The results for $\delta = 0.1$ are presented in Fig. 6. As is seen, θ changes around zero and this change increases with an increase of size asymmetry. As regards the charge asymmetry, the modulus of θ decreases with the variation of the charge asymmetry parameter ν from 0.9 to -0.9 for the fixed δ, and $|\theta|$ approaches zero for $\nu = -0.9$. In particular, for $\delta = 0.1$ the angle θ changes continuously in the range from -14° to $+16.5^\circ$ for $\nu = 0.9$ and from -0.3° to $+0.75^\circ$ for $\nu = -0.9$ when ζ is varied from 0 to 0.5. For $\delta = 0.2$ we have $-30^\circ \lesssim \theta \lesssim +44^\circ$ ($\nu = 0.9$) and $-0.03^\circ \lesssim \theta \lesssim +1.3^\circ$ ($\nu = -0.9$) in the same range of ζ. In general, the charge density fluctuations are the dominant fluctuations for $\delta < 0.3$. It should be noted that for a small size asymmetry, the λ lines associated with the periodic ordering are located at much higher temperatures than the spinodals indicating phase separation into two uniform phases.

Summarizing, in the PM with a small size asymmetry we expect the phase transition to an ionic crystal with a compact unit cell where nearest neighbors are oppositely charged, at least when ζ is sufficiently large. In particular, the CsCl crystal was observed experimentally for the system of oppositely charged colloids of comparable sizes [26]. For low volume fractions, compact charge-ordered clusters are expected, in agreement with experiments for oppositely charged proteins [9] and with simulations [27].

C. Moderate and large size asymmetry

Let us consider the case of moderate and large size asymmetry corresponding to $\delta > 0.3$ ($\lambda > 2$). In fact, PMs with $\delta = 0.3$ demonstrate a crossover-type behavior. The λ lines and the corresponding wave numbers for $\delta = 0.3$ are shown in Figs. 7 and 8, respectively. It follows from our calculations that PMs with $\delta = 0.3$ and $\nu < -0.67$ do not undergo an instability with respect to fluctuations with $k_b \neq 0$. This is contrary to the results obtained for PMs with a small size asymmetry (see Fig. 4). Similar to the small size asymmetry case, the λ-line temperature decreases when ν varies from 0.9 to -0.67. For $\nu = -0.67$, the λ line associated with $k_b \neq 0$ is located at T^* slightly lower than T^* at the spinodal indicating the separation in two uniform phases for the same ζ.

As is seen from Fig. 8, the dependence of the wave numbers x_b on the volume fraction ζ is more prominent than that shown in Fig. 5. In particular, x_b is an increasing function of ζ for $|\nu| \leqslant 0.33$. Such behavior is consistent with the decrease of the interparticle separation for decreasing average volume per particle for the same type of structure. For $\nu \geqslant 0.67$, x_b first very slowly increases and then again slowly decreases when volume fraction increases. For $\nu = -0.67$, x_b rapidly decreases. For very small values of ζ, $x_b \approx \pi$ ($l_b \approx \sigma_+ + \sigma_-$) without regard to the charge asymmetry.

The variation of the direction of strong fluctuations along the λ lines (angle θ) is shown in Fig. 9. As is seen, the charge density fluctuations still prevail over the total number density fluctuations for $-0.33 \leqslant \nu \leqslant 0.9$ except for a high-density region (see the case $\nu = 0.9$).

The fluid-solid phase coexistence in the PM with $\delta = 0.3$ and $\nu = 0$ was studied by computer simulations in Ref. [57]. In particular, it was found that there is a coexistence at $T^* = 0.033$ between a fluid at $\zeta = 0.38$ and a (NaCl) solid phase at

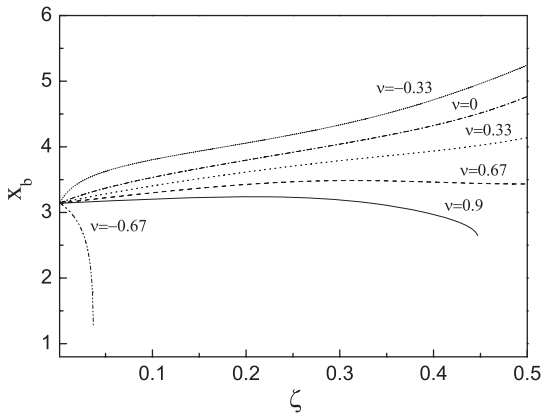

FIG. 8. The wave number $x_b = k_b\sigma_\pm$ corresponding to the ordering of ions along the λ lines shown in Fig. 7 for $\delta = 0.3$. ζ is the volume fraction of ions.

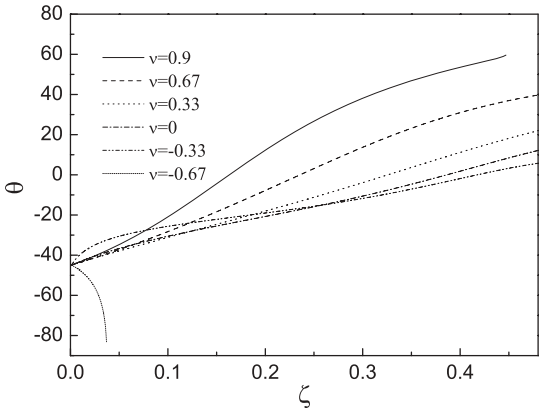

FIG. 9. The variation of angle θ along the λ lines presented in Fig. 7. θ is measured in degrees.

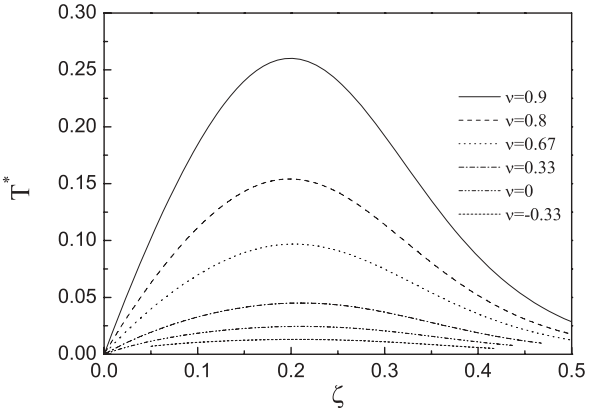

FIG. 11. The λ lines for the transition to the ordered phase for $\delta = 0.5$. Temperature T^* and the volume fraction of ions ζ are in dimensional reduced units defined in Eqs. (9) and (12), respectively.

0.51. Our calculations of the λ-line temperature corresponding to $\zeta = 0.38$ yield $T^* = 0.037$ (see Fig. 7). At this point, the order parameter is connected to the charge density fluctuations ($\theta \approx 0^\circ$) suggesting the phase transition to the ionic crystal.

For $\delta > 0.3$ all the λ lines associated with $k_b \neq 0$ demonstrate a single maximum for the volume fraction ζ_m (see Figs. 10, 11, and 14). This implies that the periodic ordering is less favorable at higher volume fractions. This behavior is similar to that found in Ref. [33] but for the higher values of δ, namely for $\delta > 0.4$. It is worth noting that the λ lines lie at temperatures lower than those found in Ref. [33]. This tendency is kept for the whole region of the variation of δ. On the other hand, the comparative analysis performed within the same regularization scheme, i.e., the WCA regularization, shows that the account of the k dependence of the reference system correlation functions leads to a pronounced increase of the λ-lines temperatures for moderate and large size asymmetry (see Fig. 10). Such a strong impact of the above-mentioned k dependence on the magnitude of the λ-lines temperatures is contrary to the results found for a one-component fluid with competing attractive and repulsive interactions [58].

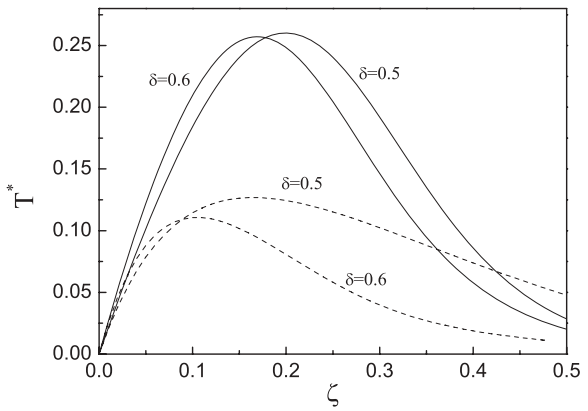

FIG. 10. The λ lines for the transition to the ordered phase for $\nu = 0.9$ and for two values of the size asymmetry ($\delta = 0.5$ and $\delta = 0.6$). Solid and dashed lines correspond to a nonlocal and local approximations for the hard-sphere reference system, respectively. Temperature T^* and the volume fraction of ions ζ are in dimensional reduced units defined in Eqs. (9) and (12), respectively.

Unlike in Ref. [33], our results demonstrate the dependence of ζ_m on the both parameters δ and ν. In general, ζ_m decreases noticeably with an increase of δ and has a nonmonotonous behavior with the variation of ν. By contrast, the maximal value of the λ-lines temperature slightly depends on the size asymmetry for $\delta > 0.3$.

Let us describe in some detail the case where $\delta = 0.5$ ($\lambda = 3$, volume ratio $\sim$30), characterizing moderate size asymmetry. $\delta = 0.5$ can be found in a solution of charged molecules of diameter $\sim$1 nm in the presence of counterions of diameter $\sim$0.3 nm, in some RTIL, or, finally, in a mixture of oppositely charged globular proteins or nanoparticles in deionized solvent.

For $\delta = 0.5$, the wave number x_b increases along the λ line from $x_b < \pi$ for $\zeta \leqslant 0.2$ to $x_b > \pi$ for $\zeta \geqslant 0.2$ except for the case of large charge asymmetry $\nu = 0.9$ (see Fig. 12). Such a behavior implies that different ordered structures can be formed with the variation of ζ. For $\nu = 0.9$, the wave number $x_b < \pi$ along the λ line ($0 \leqslant \zeta \leqslant 0.5$) and depends only slightly on the volume fraction. For $|\nu| < 0.33$, x_b change their trend sharply for the large values of ζ ($\zeta \simeq 0.4$).

The dominant field is $\rho_{\mathbf{k},N}$ at small ζ for all ν (see Fig. 13). For $\nu \geqslant 0.33$, the character of the dominant fluctuations

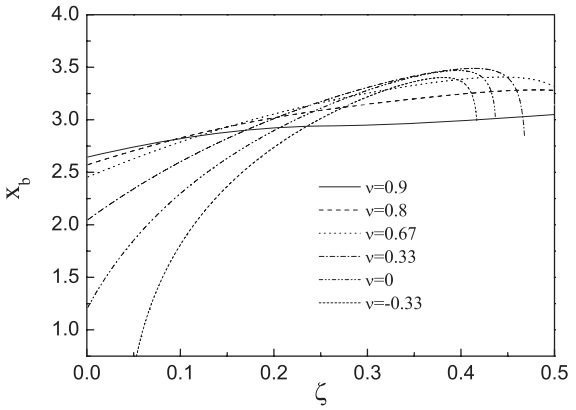

FIG. 12. The wave number $x_b = k_b\sigma_\pm$ corresponding to the ordering of ions along the λ lines shown in Fig. 11 for $\delta = 0.5$. ζ is the volume fraction of ions.

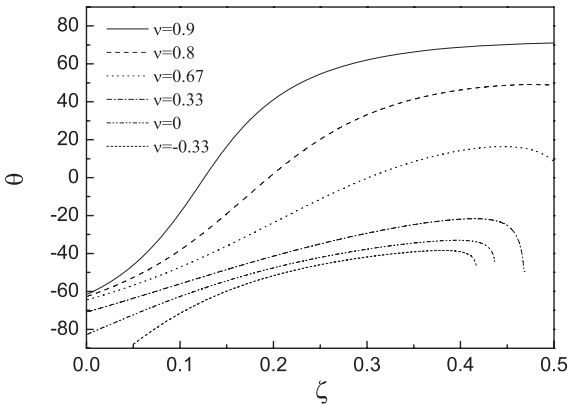

FIG. 13. The variation of angle θ along the λ lines presented in Fig. 11 for $\delta = 0.5$. θ is measured in degrees.

changes with an increase of ζ. In particular, θ varies from -61° to $+71^\circ$ for $\nu = 0.9$ and from -62° to $+49^\circ$ for $\nu = 0.8$ when the volume fraction increases from 0 to 0.5. For $\nu = 0.67$, the dominant field is $\rho_{\mathbf{k},Q}$ when $\zeta \geqslant 0.11$. For $|\nu| \leqslant 0.33$, the angle θ takes a maximum value θ_m for $\zeta \simeq 0.4$ and the modulus of θ_m increases when ν varies from 0.33 to -0.33: mod $\theta_m \simeq 22^\circ$ for $\nu = 0.33$ and mod $\theta_m \simeq 38^\circ$ for $\nu = -0.33$. Thus, the charge density fluctuations prevail over the total number density fluctuations along the λ lines for this range of ν. In general, for the intermediate size asymmetry, both the charge density and the total number density are inhomogeneous in space.

Let us focus on the large size asymmetry, $\delta > 0.6$ ($\lambda > 4$, volume ratio > 60). For $\delta \geqslant 0.6$, we obtain $x_b < \pi$ in the region $0 \leqslant \zeta \leqslant 0.5$. The λ line and the dependence of x_b on the volume fraction for $\delta = 0.8$ are shown in Figs.14 and 15. As is seen, x_b first increases, reaching its maximal value, and then decreases with the increase of ζ. The maximum becomes more pronounced with the decrease of charge asymmetry. Such behavior of x_b is typical of the systems with $0.6 \leqslant \delta \leqslant 0.9$. The variation of the angle θ along the λ lines for $\delta = 0.8$ is shown in Fig. 16. For the charge asymmetry range $0 \leqslant \nu \leqslant 0.8$, the total number density fluctuations are the dominant fluctuations along the λ lines. Moreover, the

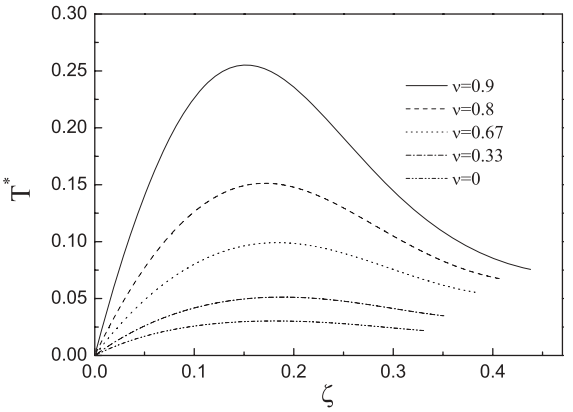

FIG. 14. The λ lines for the transition to the ordered phase for $\delta = 0.8$. Temperature T^* and the volume fraction of ions ζ are in dimensional reduced units defined in Eqs. (9) and (12), respectively.

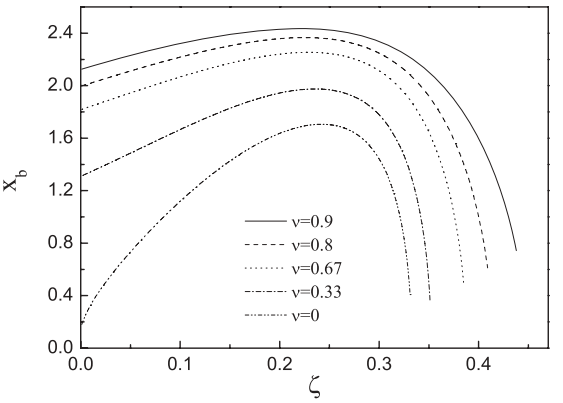

FIG. 15. The wave number $x_b = k_b\sigma_\pm$ corresponding to the ordering of ions along the λ lines shown in Fig. 14 for $\delta = 0.8$. ζ is the volume fraction of ions.

contribution from this type of fluctuations increases when the charge asymmetry decreases. For $\nu = 0.9$, the character of the dominant fluctuations changes continuously along the λ line from the total number density fluctuations for $0 \lesssim \zeta \lesssim 0.12$ to the charge density fluctuations reaching a maximal value at $\xi \simeq 0.2$. For $\zeta \gtrsim 0.28$, the dominant fluctuations are, again, the total density fluctuations. It should be noted that, for $\delta = 0.9$, the total density fluctuations play the dominant role along the whole λ line for $0 \leqslant \nu \leqslant 0.9$.

In the approximation considered, PMs with $\delta > 0.6$ and $\nu < 0$ do not undergo instabilities against the fluctuations with $k_b \neq 0$. Moreover, the λ lines tend to lower T^* with the decrease of the charge asymmetry coming close to the spinodals associated with the phase separation into uniform phases. This implies that the phase transition to the periodic ordering in the PMs with large size asymmetry becomes less favorable when the charge asymmetry decreases.

In conclusion, for the PMs with moderate and large size and charge asymmetry, we expect the phase transition to the colloid crystals of different structure formed by a nearly charge-neutral units for small and large volume fractions. The size of these units depends on the charge ratio and is generally larger than in the case of $\delta < 0.3$. For volume fractions near the maximum temperature at the λ line the number density in positively charged regions is different from the number

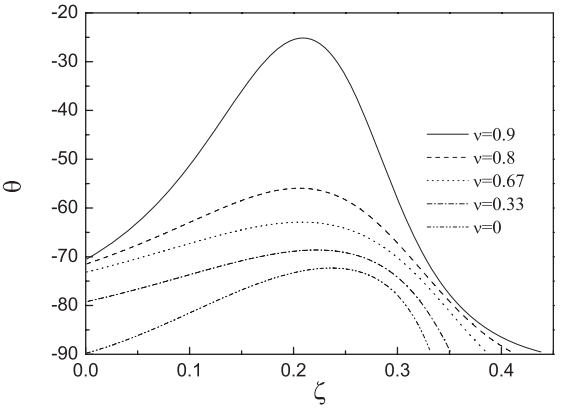

FIG. 16. The variation of angle θ along the λ lines presented in Fig. 14 for $\delta = 0.8$. θ is measured in degrees.

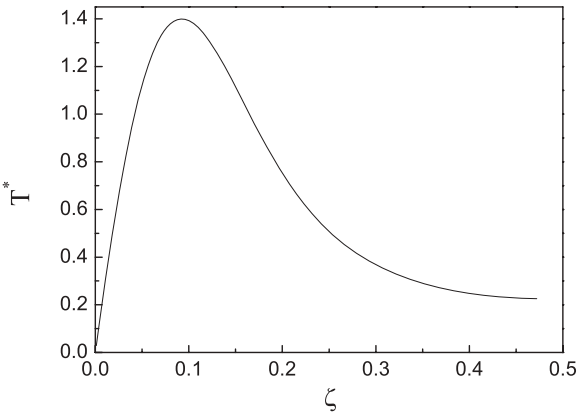

FIG. 17. The λ line for the transition to the ordered phase for $\delta = \nu = 0.99$. Temperature T^* and the volume fraction of ions ζ are in dimensional reduced units defined in Eqs. (9) and (12), respectively.

density in negatively charged regions in the fluctuation that destabilizes the homogeneous phase (see Figs. 14 and 16). Global stability, however, may correspond to another structure. For a large size asymmetry case, the complex structures discussed above may be preempted by the phase separation in two uniform phases when the charge asymmetry decreases.

D. Very large asymmetry

Let us consider the system with a very large asymmetry in size and charge: $\delta,\nu \to 1$. For $\delta = 0.99$ ($\lambda = 200$) and $\nu = 0.99$ ($Z = 200$), the λ line and the corresponding wave vectors are shown in Figs. 17 and 18. As expected, the region bounded by the λ line extends to higher temperatures in this case. The λ line assumes a maximum with the coordinates $\zeta_m \simeq 0.09$, $T_m^* \simeq 1.4$, and $k_{b,m}\sigma_\pm \simeq 2$. Remarkably, T_m^* is five times higher and ζ_m is two times lower than for $\delta = \nu = 0.9$ ($\lambda = Z = 19$). On the other hand, the above-mentioned value of T_m^* is by an order of magnitude smaller than that obtained for the same model in Ref. [33]. Recall that ζ_m has no size and charge dependence in the approximation used in the previous work. The period of the OP oscillations $l_b = 2\pi/k_b \sim \pi\sigma_+/2$ persists in the region $0 < \zeta < 0.25$ and increases for a higher

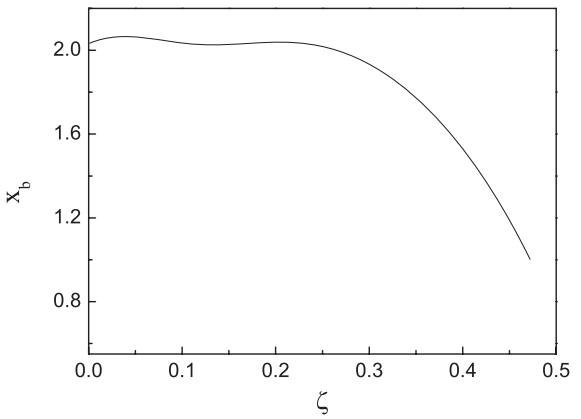

FIG. 18. The wave number $x_b = k_b\sigma_\pm$ corresponding to the ordering of ions along the λ line shown in Fig. 17. ζ is the volume fraction of ions.

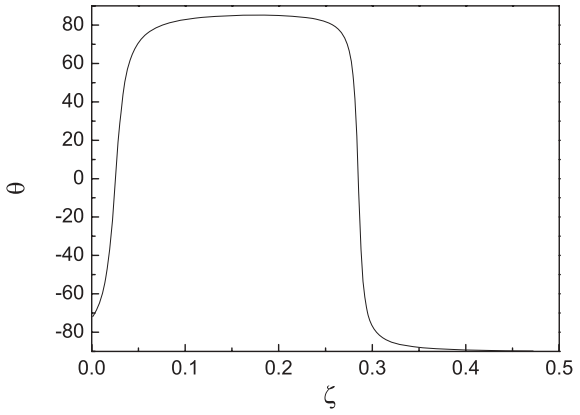

FIG. 19. The variation of the angle θ along the λ line shown in Fig. 17. θ is measured in degrees.

value of the volume fraction. The behavior of the angle θ indicating the direction of the dominant fluctuations is shown in Fig. 19. As is seen, θ changes its trend sharply from $\sim -70^\circ$ to $\sim 70^\circ$ in the region $0 \lesssim \zeta \lesssim 0.05$. Then θ remains nearly constant ($\theta \approx 80^\circ$) in a wide region of ζ ($0.05 < \zeta < 0.25$) and again changes sharply to $\sim -90^\circ$, keeping this value for $\zeta \lesssim 0.5$. We suggest that such a behavior of the OP indicates the re-entrant phase transition observed experimentally in the colloidal systems [12,13].

IV. DISCUSSION

The present analysis has shown that the size and charge asymmetry is expected to have a significant effect on the periodic ordering in the systems with dominant Coulomb interactions.

For the PM with a small size asymmetry ($\lambda < 2$), the trend of the λ lines in a wide region of the volume fractions is qualitatively similar to that found for the RPM. This is consistent with the behavior of OP demonstrating only a small deviation from the pure charge density oscillations. In this case, we expect that the ordered phase corresponding to an ionic crystal with a compact unit cell is formed at lower temperatures and at higher volume fractions when compared to the λ lines. In particular, such behavior was confirmed experimentally for the system of oppositely charged colloidal particles of comparable sizes (see Ref. [26]). On the other hand, we expect that charge-ordered living clusters are formed in the fluid phase with the period of the charge wave similar to the one in the crystal. It is worth noting that in the case of moderate and small charge asymmetry, the trends of the λ lines deviate from the RPM-like behavior when the volume fraction increases.

PMs with $\lambda = 2$ show a crossover-type behavior between the regime of small size asymmetry and the regime of moderate and large size asymmetry. In qualitative agreement with the results of Ref. [57], our results predict the phase transition to the ionic crystal for the system with $\lambda = 2$ and $Z = 1$.

For a moderate and large size asymmetry ($2 < \lambda < 20$), the λ lines show a single maximum T_m^* at volume fraction ζ_m. While T_m^* depends slightly on the size asymmetry, ζ_m decreases noticeably when the size asymmetry increases. In addition, T_m^* decreases with the decrease of charge asymmetry.

The nonmonotonic temperature at the λ line indicates that some kind of a crystalline phases can be stable for intermediate volume fractions, and re-entrant melting occurs at the high volume fractions (where the temperature at the λ line decreases). It should be noted that both the charge density and the total number density oscillate along the λ lines and their contributions to the OP vary depending on the charge asymmetry as well as on the volume fraction. Note that for overall charge neutrality the number of negatively charged species is Z times larger than the number of positively charged species. For a large charge asymmetry the main contribution to the number density comes from the negatively charged species.

The expected phase transition to the crystal phase of different structure is in qualitative agreement with the simulation studies which predict different crystal structure in mixtures of large and small oppositely charged spherical colloids with $\lambda \simeq 3$ [18,26]. Remarkably, three of the predicted structures were also observed experimentally [18,26]. Our results also show that the large nearly neutral clusters may be formed in the PMs with a moderate and large size asymmetry at the small volume fractions. Such a behavior was observed experimentally in water solutions of the charged globular proteins [8]. On the other hand, the appearance of instabilities in the fluid phase against the periodic ordering for a moderate size and charge asymmetry may explain to some extent the inhomogeneous structure observed in RTILs. In these cases the role of non-Coulomb interactions should be clarified in future studies. The trend of the λ lines found for the large size asymmetry implies that the periodic ordering becomes less favorable when the charge asymmetry decreases and the fluid-solid phase transition may be preempted by the phase separation in two uniform phases when the charge asymmetry decreases.

For a very large size and charge asymmetry ($\lambda = Z = 200$) the number density fluctuations dominate except for small ranges of ζ (Fig. 19). The period of the OP oscillations depends very slightly on ζ in the region $0 < \zeta < 0.25$ (Fig. 18). In this case, the clusters with diameter $\sim \pi\sigma_+/2 \approx 1.5\sigma_+$ are formed. Each cluster is composed of a large positive (negative) ion surrounded by a narrow layer of compensating negative (positive) charges. Such clusters are associated with pretransitional ordering—they are present in the solution when the transition to the crystal is approached. Stability analysis alone is not sufficient for determination of the crystalline structure. We can expect formation of the colloidal crystal with periodic distribution of particles surrounded by a cloud of counterions for very small volume fractions. It should be noted that at the point of the λ line corresponding to $\zeta = 0.05$ the inverse screening length is $\kappa\sigma_+ \approx 0.7$. The screening increases with the increase of ζ, indicating the reduction of the long-range repulsion along the λ line. For $0.1 < \zeta < 0.2$ we find $\theta > 80$, and the OP consists of almost pure number density wave with the wavelength $\approx 1.5\sigma_+$, with negligible periodic ordering of the charge density (see Fig. 19). We thus may conclude that nearly charge-neutral units composed of the particle surrounded by a thin layer of the neutralizing counterions are formed. Crystal formation of neutral (thus, noninteracting) units is not expected if their volume fraction is $\zeta \sim 0.1$. Thus, a re-entrant melting could be expected in this region. For $\zeta > 0.25$, we find decreasing θ and the OP consists of both the number and the charge waves. The period of the OP oscillations increases with the increase of the volume fraction. Such a behavior may indicate the ion rearrangement leading to the formation of larger clusters.

In experiments a fluid–bcc crystal–fluid phase coexistence was found with an increase of the colloid volume fraction [12,13]. The dilute fluid–dilute crystal–dense fluid–dense crystal transitions, for increasing ζ, with the re-entrant melting for $\zeta \sim 0.1$ were also seen [11]. In the latter experiment room temperature in our reduced units is $T^* \approx 0.39$. For $0.1 < \zeta < 0.2$, the reduced temperature at the λ line is much higher than 0.39, and further studies are necessary for comparison between our theory and experiment. Nevertheless, we can make an observation that crystal phases were observed for the volume fractions corresponding to the OP consisting of both the number and the charge density waves, and the re-entrant melting was observed when the OP consists only of the number density wave, with no charge inhomogeneity.

V. CONCLUDING REMARKS

In this paper we have used the CVs-based theory to study the periodic ordering in the PMs with size and charge asymmetry. We consider the Gaussian approximation of the functional of the grand partition function which, in turn, leads to the free energy and the direct correlation functions in the RPA. Using analytic expressions for direct correlation functions in the RPA, we study the effects of the size and charge asymmetry on the instabilities of the uniform phase with respect to the periodic ordering.

We determine the CV associated with the OP. To this end, we diagonalize the square form of the Hamiltonian and analyze the behavior of the eigenvalues. This enables us to identify the OP connected with the periodic ordering and determine the character of the dominant fluctuations along the λ lines.

We extend the study undertaken in Ref. [33] by introducing several modifications. We take into account the dependence of the reference hard-sphere correlation functions on the wave vectors and adopt the WCA regularization of the Coulomb potential inside the hard core. While the latter leads to a significant decrease of the λ-line temperatures, the former gives rise to their increase for the same regularization scheme. The combination of the above-mentioned modifications gives rise to λ-line temperatures much lower than those found in Ref. [33]. A similar situation holds for the whole range of diameter, λ, and charge, Z, ratios of the two ionic species. Besides, the WCA regularization scheme leads to the higher values of the wave vectors k_b (smaller $l_b = 2\pi/k_b$) associated with the λ line when compared to Ref. [33]. Precise values of k_b cannot be determined in a perturbative approach, since the regularization of the Coulomb potential is not unique.

According to a typical behavior of the λ lines, we distinguish three regimes: the regime of small size asymmetry ($\lambda < 2$), the regime of moderate and large charge asymmetry ($2 < \lambda < 20$) and the regime of very large size and charge asymmetry ($\lambda = \nu = 200$). As is seen, the first regime is found to be narrower than that considered in the previous work. Remarkably, the qualitative dependence on the charge

asymmetry appears in the first regime: For a small charge asymmetry, the λ lines T^* versus ζ demonstrate the departure from the monotonously increasing behavior which becomes more evident with an increase of λ. This change in the phase diagram is directly related to the nonlocal approximation used for the reference hard-sphere system. Unlike Ref. [33], our results also show that the models with $\lambda \geqslant 4$ and $Z < 1$ (a large charge at the smaller ion) do not undergo the instabilities with respect to the periodic ordering in the whole region of ζ. Thus, we can state that the modifications introduced in this paper have led to quantitative and partly qualitative changes in the phase diagram obtained in Ref. [33]

We conclude that both the size and charge asymmetry affect the periodic ordering in the systems with dominant Coulomb interactions, namely (1) for $\lambda < 2$, the charge density oscillations dominate in the OP—the phase transition to an ionic crystal with a compact unit cell is expected; (2) for $\lambda > 2$, both the charge density and the total number density oscillate along the structural line and their contributions to the OP depend on λ and Z; (3) for a moderate and large λ, a crystalline phase can be stable for intermediate volume fractions and re-entrant melting occurs at high volume fractions, the large nearly neutral clusters may be formed at small volume fractions; (4) for a large λ and small Z, the fluid-crystal phase transition can be preempted by the gas-liquid-like phase separations; (5) for a very large λ and Z, the colloidal crystal with periodic distribution of particles surrounded by a cloud of counterions is expected for very small volume fractions and a re-entrant melting for the higher volume fractions.

The RPA predicts only the existence of a region in which a model ionic fluid is unstable with respect to the OP oscillations associated with the periodic ordering. In this context, our phase diagrams indicate the pretransitional effects. The fluctuation effects of the higher order than the second order should be taken into account in order to get the information on both the more precise location of the phase diagrams and the pattern shapes which can be formed. This will be done elsewhere.

ACKNOWLEDGMENTS

Partial support by the Ukrainian-Polish joint research project under the Agreement on Scientific Collaboration between the Polish Academy of Sciences and the National Academy of Sciences of Ukraine for 2009–2011 is gratefully acknowledged. A part of this work was realized within the International Ph.D. Projects Programme of the Foundation for Polish Science, cofinanced from European Regional Development Fund within Innovative Economy Operational Programme "Grants for innovation." The work of O.P. was partially supported by the Special Program of Fundamental Research of the Division of Physics and Astronomy of the National Academy of Sciences of Ukraine (No. 0112U003119).

APPENDIX

1. Explicit expressions for the coefficients t_{IJ}

$$t_{NN} = \frac{a_{22}(k)}{\Delta}, \quad t_{NQ} = -\frac{a_{12}(k)}{\Delta}, \qquad t_{QN} = -\frac{a_{21}(k)}{\Delta}, \quad t_{QQ} = \frac{a_{11}(k)}{\Delta}, \tag{A1}$$

where

$$a_{11}(k) = \frac{1}{\sqrt{1+\alpha_1^2}}, \quad a_{12}(k) = \frac{1}{\sqrt{1+\alpha_2^2}}, \qquad a_{21}(k) = \frac{\alpha_1}{\sqrt{1+\alpha_1^2}}, \quad a_{22}(k) = \frac{\alpha_2}{\sqrt{1+\alpha_2^2}}, \tag{A2}$$

$$\Delta = a_{11}a_{22} - a_{12}a_{21} = \frac{|\tilde{\mathcal{C}}_{NQ}(k)|}{\tilde{\mathcal{C}}_{NQ}(k)}, \tag{A3}$$

$$\alpha_{1,2}(k) = \frac{\tilde{\mathcal{C}}_{QQ}(k) - \tilde{\mathcal{C}}_{NN}(k) \pm \sqrt{[\tilde{\mathcal{C}}_{NN}(k) - \tilde{\mathcal{C}}_{QQ}(k)]^2 + 4\tilde{\mathcal{C}}_{NQ}(k)^2}}{2\tilde{\mathcal{C}}_{NQ}(k)}. \tag{A4}$$

[1] G. Stell, J. Stat. Phys. **78**, 197 (1995).
[2] Y. Levin and M. F. Fisher, Physica A **225**, 164 (1996).
[3] W. Schröer, in *Ionic Soft Matter: Modern Trends and Applications*, NATO ASI Series II, edited by D. Henderson, M. Holovko, and A. Trokhymchuk (Springer, Dordrecht, 2004), p. 143.
[4] W. Schröer, Contrib. Plasma Phys. **52**, 78 (2012).
[5] A. Z. Panagiotopoulos, J. Phys.: Condens. Matter **17**, S3205 (2005).
[6] A.-P. Hynninen and A. Z. Panagiotopoulos, Mol. Phys. **106**, 2039 (2008).
[7] O. Russina, A. Triolo, L. Gotrani, and R. Caminiti, J. Phys. Chem. Lett. **3**, 27 (2011).
[8] A. Stradner, H. Sedgwick, F. Cardinaux, W. C. K. Poon, S. U. Egelhaaf, and P. Schurtenberger, Nature **432**, 492 (2004).
[9] Y. Desfougeres, T. Croguennec, V. Lechevallier, S. Bouhallab, and F. Nau, J. Phys. Chem. B **114**, 4138 (2010).
[10] A. K. Arora, B. V. R. Tata, A. K. Sood, and R. Kesavamoorthy, Phys. Rev. Lett. **60**, 2438 (1988).
[11] D. El Masri, T. Vissers, S. Badaire, J. C. P. Stiefelhagen, H. Rao Vutukuri, P. Helfferich, T. H. Zhang, W. K. Kegel, A. Imhof, and A. van Blaaderen, Soft Matter **8**, 6979 (2012).
[12] J. Yamanaka, H. Yoshida, T. Koga, N. Ise, and T. Hashimoto, Phys. Rev. Lett. **80**, 5806 (1998).
[13] C. P. Royall, M. E. Leunissen, A. P. Hynninen, M. Dijkstra, and A. van Blaaderen, J. Chem. Phys. **124**, 244706 (2004).
[14] A. Ciach, W. T. Góźdź, and G. Stell, J. Phys.: Condens. Matter **18**, 1629 (2006)
[15] F. Stillinger and R. Lovett, J. Chem. Phys. **48**, 3858 (1968).
[16] A. Ciach and O. Patsahan, Phys. Rev. E **74**, 021508 (2006).
[17] C. Vega, F. Bresme, and J. L. F. Abascal, Phys. Rev. E **54**, 2746 (1996).

[18] A. P. Hynninen, M. E. Leunissen, A. van Blaaderen, and M. Dijkstra, Phys. Rev. Lett. **96**, 018303 (2006).
[19] J. Weis, D. Levesque, and J. Caillol, J. Chem. Phys. **109**, 7486 (1998).
[20] E. Spohr, B. Hribar, and V. Vlachy, J. Phys. Chem. B **106**, 2343 (2002).
[21] J. M. Romero-Enrique, G. Orkoulas, A. Z. Panagiotopoulos, and M. E. Fisher, Phys. Rev. Lett. **85**, 4558 (2000).
[22] Q. Yan and J. J. de Pablo, Phys. Rev. Lett. **86**, 2054 (2001).
[23] F. Bresme and J. Alejandre, J. Chem. Phys. **118**, 4134 (2003).
[24] J. B. Caballero, E. G. Noya, and C. Vega, J. Chem. Phys. **127**, 244910 (2007).
[25] C. Vega, E. Sanz, J. L. F. Abascal, and E. G. Noya, J. Phys.: Condens. Matter **20**, 153101 (2008).
[26] M. E. Leunissen, C. G. Christova, A. P. Hynninen, C. P. Royall, A. I. Campbell, A. Imhof, M. Dijkstra, R. van Roij, and A. van Blaaderen, Nature **437**, 235 (2005).
[27] P. M. Biesheuvel, S. Lindhoud, R. de Vries, and M. A. Cohen Stuart, Langmuir **22**, 1291 (2006).
[28] A. Shukla, E. Mylonas, E. di Cola, S. Finet, P. Timmins, T. Narayanan, and D. I. Svergun, Proc. Natl. Acad. Sci. USA **105**, 5075 (2008).
[29] P. Kowalczyk, A. Ciach, P. A. Gauden, and A. P. Terzyk, J. Colloid Interf. Sci. **363**, 579 (2011).
[30] L. Harnau and J.-P. Hansen, J. Chem. Phys. **116**, 9051 (2002).
[31] S. Kondrat, M. Bier, and L. Harnau, J. Chem. Phys. **132**, 184901 (2010).
[32] G. C. Ganzenmüller and G. N. Patey, Phys. Rev. Lett. **105**, 137801 (2010).
[33] A. Ciach, W. T. Góźdź, and G. Stell, Phys. Rev. E **75**, 051505 (2007).
[34] A. Ciach and G. Stell, Int. J. Mod. Phys. B **19**, 3309 (2005).
[35] Y. Rosenfeld, Phys. Rev. Lett. **63**, 980 (1989).
[36] J. L. Lebowitz, Phys. Rev. **133**, A895 (1964).
[37] J. D. Weeks, D. Chandler, and H. C. Andersen, J. Chem. Phys. **54**, 5237 (1971).
[38] D. Chandler and H. C. Andersen, J. Chem. Phys. **54**, 26 (1971).
[39] O. V. Patsahan, Condens. Matter Phys. **7**, 35 (2004).
[40] O. V. Patsahan, Physica A **272**, 358 (1999).
[41] O. V. Patsahan and T. M. Patsahan, J. Stat. Phys. **105**, 285 (2001).
[42] D. N. Zubarev, Dokl. Acad. Nauk SSSR **95**, 757 (1954). [in Russian].
[43] I. R. Yukhnovsky, Zh. Eksp. Teor. Fiz. **34**, 379 (1958) [Sov. Phys. – JETP **34**, 263 (1958)].
[44] I. R. Yukhnovskii, *Phase Transition of the Second Order: Collective Variables Method* (World Scientific, Singapore, 1987).
[45] O. Patsahan and I. Mryglod, Condens. Matter Phys. **9**, 659 (2006).
[46] O. V. Patsahan and T. M. Patsahan, Phys. Rev. E **81**, 031110 (2010).
[47] O. V. Patsahan, I. M. Mryglod, and T. M. Patsahan, J. Phys.: Condens. Matter **18**, 10223 (2006).
[48] O. V. Patsahan and I. M. Mryglod, J. Phys. A **39**, L583 (2006).
[49] A. Ciach, Phys. Rev. E **78**, 061505 (2008).
[50] A. Ciach and W. T. Góźdź, Condens. Matter Phys. **13**, 23603 (2010).
[51] N. W. Ashcroft and D. C. Langreth, Phys. Rev. **156**, 685 (1967).
[52] N. W. Ashcroft and D. C. Langreth, Phys. Rev. **166**, 934 (1968).
[53] A. Ciach and G. Stell, J. Mol. Liq. **87**, 255 (2000).
[54] O. V. Patsahan and I. M. Mryglod, Condens. Matter Phys. **7**, 755 (2004).
[55] J.-M. Caillol, J. Stat. Phys. **115**, 1451 (2004).
[56] J.-M. Caillol, Mol. Phys. **103**, 1271 (2005).
[57] A.-P. Hynninen and A. Z. Panagiotopoulos, J. Phys.: Condens. Matter **21**, 465104 (2009).
[58] A. J. Archer, C. Ionescu, D. Pini, and R. Reatto, J. Phys.: Condens. Matter **20**, 415106 (2008).